Herpesvirus-mediated stabilization of ICP0 expression neutralizes restriction by TRIM23

Xing Liu[a], Dhiraj Acharya[b], Eric Krawczyk[a], Chase Kangas[a], Michaela U. Gack[b], and Bin He[a,1]

[a]Department of Microbiology and Immunology, University of Illinois College of Medicine, Chicago, IL 60612; and [b]Florida Research and Innovation Center, Cleveland Clinic, Port Saint Lucie, FL 34987

Edited by Thomas Shenk, Princeton University, Princeton, NJ; received July, 15, 2021; accepted November 8, 2021

Herpes simplex virus (HSV) infection relies on immediate early proteins that initiate viral replication. Among them, ICP0 is known, for many years, to facilitate the onset of viral gene expression and reactivation from latency. However, how ICP0 itself is regulated remains elusive. Through genetic analyses, we identify that the viral $\gamma_1$34.5 protein, an HSV virulence factor, interacts with and prevents ICP0 from proteasomal degradation. Furthermore, we show that the host E3 ligase TRIM23, recently shown to restrict the replication of HSV-1 (and certain other viruses) by inducing autophagy, triggers the proteasomal degradation of ICP0 via K11- and K48-linked ubiquitination. Functional analyses reveal that the $\gamma_1$34.5 protein binds to and inactivates TRIM23 through blockade of K27-linked TRIM23 autoubiquitination. Deletion of $\gamma_1$34.5 or ICP0 in a recombinant HSV-1 impairs viral replication, whereas ablation of TRIM23 markedly rescues viral growth. Herein, we show that TRIM23, apart from its role in autophagy-mediated HSV-1 restriction, down-regulates ICP0, whereas viral $\gamma_1$34.5 functions to disable TRIM23. Together, these results demonstrate that posttranslational regulation of ICP0 by virus and host factors determines the outcome of HSV-1 infection.

herpes simplex virus | viral replication | gene expression | TRIM23 | virus–host interaction

Herpes simplex viruses (HSV) are human pathogens that switch between lytic and latent infections intermittently (1, 2). This is a lifelong source of infectious viruses (1, 2), in which immediate early proteins drive the onset of HSV replication. Among them, ICP0 enables viral gene expression or reactivation from latency (2–4), which involves chromatin remodeling of the HSV genome, resulting in de novo virus production. In this process, the accessory factor $\gamma_1$34.5 of HSV is thought to govern viral protein synthesis (5, 6). It has long been known that $\gamma_1$34.5 precludes translation arrest mediated by double-stranded RNA–dependent protein kinase PKR (7–9). The $\gamma_1$34.5 protein has also been shown to dampen intracellular nucleic acid sensing, inhibit autophagy, and facilitate virus nuclear egress (10–17). In experimental animal models, wild-type HSV, but not HSV that lacks the $\gamma_1$34.5 gene, replicates competently, penetrates from the peripheral tissues to the nervous system and reactivates from latency (18–23). Despite these observations, active HSV replication or reactivation from latency is not readily reconciled by the currently known functions of the $\gamma_1$34.5 protein (8–13, 16, 17).

Several lines of work demonstrate that tripartite motif (TRIM) proteins regulate innate immune signaling and cell intrinsic resistance to virus infections (24, 25). These host factors typically work as E3 ubiquitin ligases that can synthesize degradative or nondegradative ubiquitination on viral or host proteins. A number of TRIM proteins, for example TRIM5α, TRIM19, TRIM21, TRIM22, and TRIM43, act at different steps of virus replication and subsequently inhibit viral production (26–32). Recent evidence indicates that TRIM23 limits the replication of certain RNA viruses and DNA viruses, including HSV-1 (33). In doing so, TRIM23 recruits TANK-binding kinase 1 (TBK1) to autophagosomes, thus promoting TBK1-mediated phosphorylation and activation of the autophagy receptor p62 and ultimately leading to autophagy. It is unknown whether TRIM23 plays an additional role(s) in HSV infection.

Here, we report that ICP0 expression is regulated by the $\gamma_1$34.5 protein and TRIM23 during HSV-1 infection. We show that TRIM23 facilitates the proteasomal degradation of ICP0, whereas viral $\gamma_1$34.5 maintains steady-state ICP0 expression by preventing K27-linked TRIM23 autoubiquitination that is required for TRIM23 activation. The $\gamma_1$34.5 protein also interacts with and stabilizes ICP0, enabling productive infection. Furthermore, we provide evidence that TRIM23 binds to ICP0 and induces its K11-linked polyubiquitination, which triggers K48-linked polyubiquitin-dependent proteasomal degradation of ICP0. These insights establish a model of posttranslational networks in which virus- and host-mediated mechanisms regulate immediate early protein ICP0 stability and thereby lytic HSV replication.

Results

HSV $\gamma_1$34.5 Stabilizes Immediate Early Protein ICP0 Expression. To identify the characteristics of HSV replication, we compared the replication kinetics of wild-type HSV-1 and recombinant R3616 that lacks the $\gamma_1$34.5 gene. In mouse embryonic fibroblasts (MEFs) (Fig. 1*A*), wild-type HSV-1, with a transient pause, grew steadily over the course of infection, reaching 4×10^5 pfu/mL at 72 h post infection. In contrast, the mutant R3616 virus replicated poorly. As virus infection progressed, this mutant virus grew only to 8×10^1 pfu/mL. Notably, viral

Significance

Herpes simplex viruses (HSV) can switch between lytic and latent infections, which are lifelong sources of recurrent diseases. In this process, the immediate early protein ICP0 crucially drives herpesvirus gene expression or reactivation from latency. The regulatory network of ICP0 expression is, however, largely obscure. We uncover that the HSV-1 virulence factor $\gamma_1$34.5 interacts with and stabilizes ICP0. We also demonstrate that TRIM23, a cellular E3 ligase, triggers proteasomal degradation of ICP0 in the absence of $\gamma_1$34.5. As such, removal of $\gamma_1$34.5 or ICP0 from HSV-1 cripples viral growth, whereas ablation of TRIM23 restores viral production. These findings provide a framework of virus–host regulatory circuits, which may help in the rational design of antiviral or oncolytic therapeutics.

Author contributions: X.L. and B.H. designed research; X.L., D.A., E.K., and C.K. performed research; X.L., D.A., E.K., C.K., M.U.G., and B.H. analyzed data; and X.L., D.A., M.U.G., and B.H. wrote the paper.

The authors declare no competing interest.

This article is a PNAS Direct Submission.

[1]To whom correspondence may be addressed. Email: tshuo@uic.edu.

This article contains supporting information online at http://www.pnas.org/lookup/suppl/doi:10.1073/pnas.2113060118/-/DCSupplemental.

Published December 13, 2021.

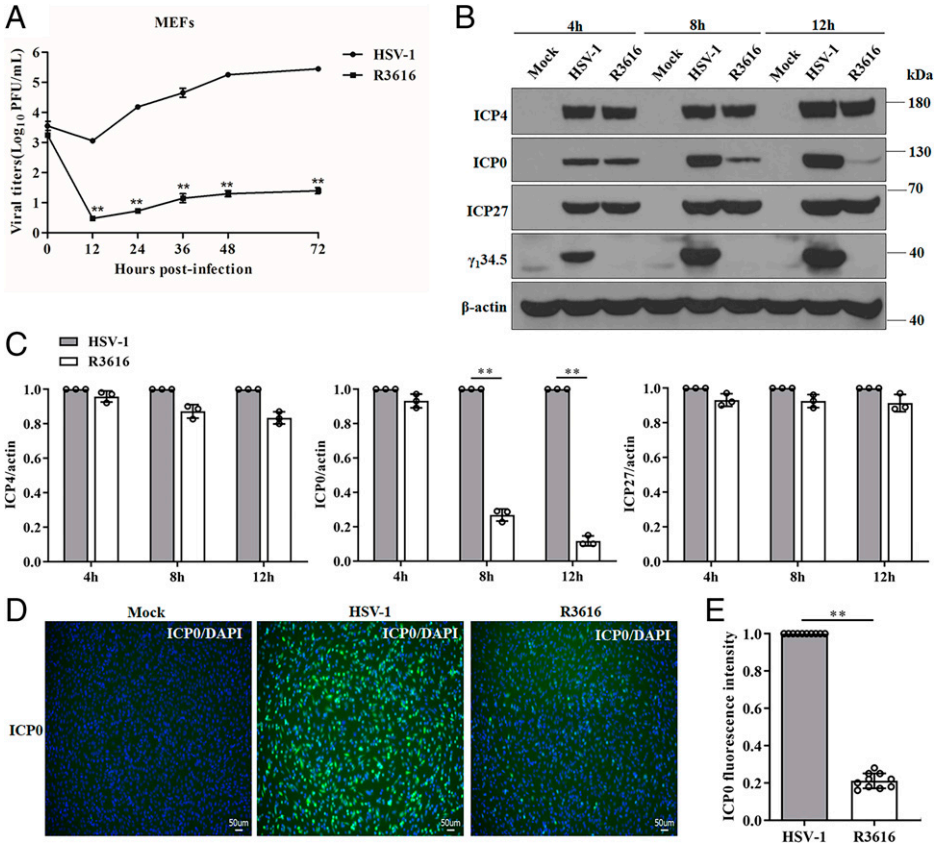

Fig. 1. HSV-1 $\gamma_1$34.5 is necessary for the expression of immediate early protein ICP0. (*A*) Kinetics of viral growth in MEFs. Cells were infected with wild-type HSV-1 or the $\gamma_1$34.5 null virus (R3616) at an MOI of 0.01, and the total virus yields were determined by plaque assay on Vero cells. (*B*) Expression of ICP4, ICP0, and ICP27. MEFs were mock infected or infected with HSV-1 or R3616 (MOI = 5). At the indicated time points, cells were harvested for Western blot analysis using antibodies against ICP4, ICP0, ICP27, $\gamma_1$34.5, and β-actin. (*C*) Quantification of ICP4, ICP0, and ICP27 in virus infection. ICP4, ICP0, and ICP27, as represented in *B*, were quantified using NIH ImageJ software and normalized to β-actin. Relative protein levels from R3616 and HSV-1 were compared. (*D*) IF analysis of ICP0. MEFs were mock infected or infected with HSV-1 or R3616 (MOI = 5) for 8 h and then stained with the ICP0 antibody (green) and DAPI (blue). Images are representative of at least 10 different areas. (*E*) Quantification of ICP0 median fluorescence intensity per cell between HSV-1 and R3616 groups. IF images in *D* were quantified using NIH ImageJ software (with the HSV-1 group as 1.0). Unpaired Student's *t* test was used for *A*, $^{**}P < 0.01$, and one-way ANOVA was used for *C* and *E*, $^{**}P < 0.01$. Data are expressed as means ± SD ($n = 3$) in *A* and *C*. Data are from quantification of at least an average 10 images per group in *E*. The data are representative of results from three independent experiments for *A* and *B*. The images are representative of results from at least 10 images for *D*.

production in cells infected with R3616 declined steeply to a barely detectable level by 12 h post infection. Furthermore, in human lung fibroblasts, wild-type virus and R3616 displayed similar phenotypes (*SI Appendix*, Fig. S2*A*). The distinct kinetics of viral growth suggests a requirement of the $\gamma_1$34.5 gene, possibly in the early stage of HSV replication.

HSV replication proceeds in a temporal manner in which immediate early proteins coordinately control subsequent viral gene expression (1, 2). Among them, ICP0, ICP4, and ICP27 drive transactivation of HSV genes for lytic infection. Furthermore, ICP0 regulates reactivation from latency. To test whether $\gamma_1$34.5 impacts immediate early gene expression, we analyzed ICP0, ICP4, and ICP27 protein abundances in virus-infected cells. As shown in Fig. 1*B*, ICP4 and ICP27 were expressed to similar levels in MEF cells infected with wild-type HSV-1 or R3616. Remarkably, ICP0 expression exhibited a different pattern. While at 4 h postinfection, similar levels of ICP0 expression were detected for wild-type HSV-1 and R3616, the levels of ICP0 increased steadily in cells infected with wild-type HSV-1. In contrast, ICP0 expression was diminished in cells infected with R3616 at 8 h and 12 h postinfection. Indeed, deletion of $\gamma_1$34.5 led to a >80% reduction in ICP0 expression but had a marginal effect on ICP4 and ICP27 abundances (Fig.1*C*). Consistently, immunofluorescence (IF) microscopy revealed notable ICP0 expression with wild-type virus but less so with R3616 (Fig. 1 *D* and *E*). As expected, similar levels of ICP4 and ICP27 were detected for wild-type HSV-1 and R3616 by IF analysis (*SI Appendix*, Fig. S1 *A–D*). To further confirm these results, we analyzed the replication of wild-type HSV-1 and R3616 in human lung fibroblasts. As seen in MEFs, the levels of ICP0 expression coincided with the presence of $\gamma_1$34.5, although with different kinetics (*SI Appendix*, Fig. S2 *B* and *C*). Together, these results show that $\gamma_1$34.5 stabilizes or enhances the expression of the immediate early protein ICP0 and promotes HSV replication.

The $\gamma_1$34.5 Protein Prevents Proteasomal Degradation of ICP0. We asked whether HSV $\gamma_1$34.5 regulates ICP0 expression at the transcription level. For this, we analyzed the abundance of RNA transcripts of ICP0, ICP4, and ICP27 in virus-infected cells. We noted that the mRNA levels of ICP0, ICP4, and ICP27 were similar in cells infected with wild-type HSV-1 or R3616 as determined by qPCR analysis (Fig. 2*A*). Under these conditions, reduced protein expression was detectable for ICP0 in cells only infected with R3616 (Fig. 2*B*). This, however, was not a general defect in viral protein expression as the levels of ICP4 and ICP27 remained unaffected. These data support that HSV $\gamma_1$34.5 regulates the steady-state level of ICP0 protein but not its RNA transcript.

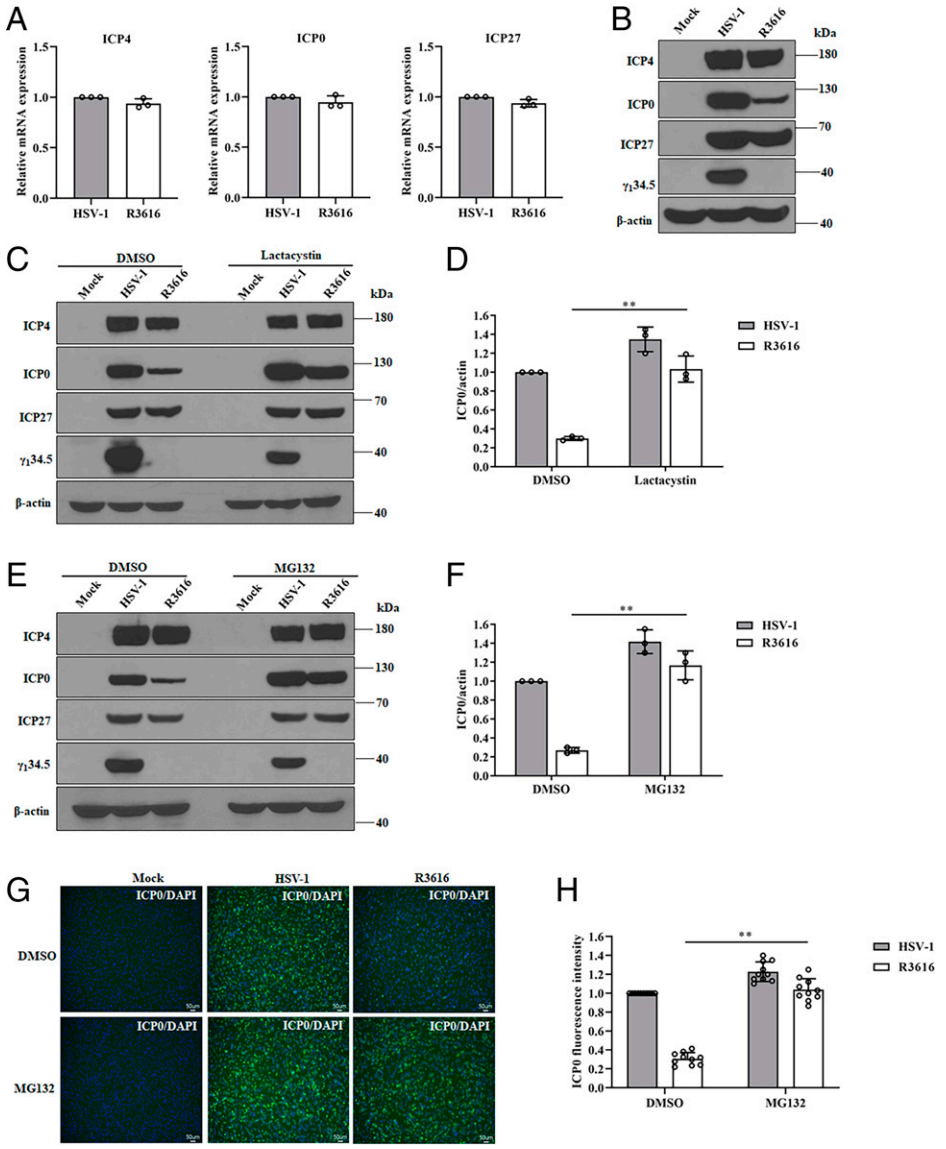

Fig. 2. The $\gamma_1$34.5 protein blocks proteasomal degradation of ICP0. (*A*) Expression of ICP4, ICP0, and ICP27 transcripts. MEFs were infected with wild-type HSV-1 or R3616 at an MOI of 5 for 8 h and then harvested for RNA extraction and qRT-PCR analysis. (*B*) Protein expression of ICP4, ICP0, and ICP27. MEFs infected as in *A* were harvested for Western blot determination with antibodies against ICP4, ICP0, ICP27, $\gamma_1$34.5, and β-actin antibodies. (*C*) Effect of lactacystin on ICP0 expression. MEFs were mock infected or infected with HSV-1 or R3616 (MOI = 5) for 2 h and then treated with DMSO or lactacystin (20 μM). At 8 h post infection, expression of ICP4, ICP0, ICP27, $\gamma_1$34.5, and β-actin were examined by Western blot analysis. (*D*) Quantification of ICP0 in control and lactacystin groups. Levels of ICP0, as illustrated in *C*, were quantified and normalized to β-actin. Relative protein levels from R3616 and HSV-1 were compared. (*E*) Effect of MG132 on ICP0 expression. Virus infection and Western blot analysis of indicated proteins were done as in *C* but with treatment of MG132 (20 μM). (*F*) Quantification of ICP0 in control and MG132 groups. (*G*) IF analysis of ICP0. MEFs were mock infected or infected with HSV-1 or R3616 (MOI = 5) for 2 h and then treated with DMSO or MG132 (20 μM). At 8 h post infection, cells were stained with the ICP0 antibody (green) and DAPI (blue). (*H*) Quantification of ICP0 median fluorescence intensity treated with DMSO or MG312. IF images in *G* were quantified using NIH ImageJ software (with the HSV-1 group as 1.0). One-way ANOVA was used for *A*, *D*, *F*, and *H*, $^{**}P < 0.01$ (one-way ANOVA). Data are expressed as means ± SD ($n = 3$) in *A*, *D*, *F*, and quantified from at least an average 10 images per group in *H*. The data are representative of results from three independent experiments for *A*, *B*, *C*, and *E*. The images are representative of results from at least 10 images for *G*.

To determine whether HSV $\gamma_1$34.5 stabilizes ICP0 protein, we evaluated the impact of pharmacological inhibitors on ICP0 protein abundance in infected cells. We first examined lactacystin, which binds to and inhibits the proteasome subunit X/MB1 (34). In MEF cells treated with vehicle (dimethyl sulfoxide [DMSO]), expression of the ICP0 protein was reduced by 70% upon infection with R3616 (Fig. 2 *C* and *D*). Treatment of cells with lactacystin restored ICP0 expression to a significant level (>70%). Although no effects were seen on ICP4 and ICP27, lactacystin apparently prevented the degradation of ICP0. To confirm this result, we assessed MG132, which potently inhibits the 26S complex of the proteasome. Immunoblot analysis showed that MG132 recovered ∼80% of ICP0 in cells infected with R3616 for 8 h as compared to infected cells treated with the vehicle control (Fig. 2 *E* and *F*). IF analysis indicated that unlike the control, MG132 increased the expression of ICP0 by >70% upon infection with R3616 (Fig. 2 *G* and *H*). These phenotypes were also seen at late time points of infection (*SI Appendix*, Fig. S3 *A–D*). To determine whether additional pathways control ICP0 expression, we measured the impact of chloroquine (lysosomal inhibitor), 3-Methyladenine (autophagy inhibitor), bafilomycin A1 (autophagy inhibitor), and Z-VAD

(pan-caspase inhibitor) but found little or a marginal effect (*SI Appendix*, Fig. S4 *A–D*). In addition, knockout of cellular TBK1 or deletion of the Us11 gene in HSV-1 did not affect ICP0 expression (*SI Appendix*, Fig. S5 *A* and *B*). These results suggest that $\gamma_1$34.5 functions to inhibit the proteasomal degradation of ICP0.

The $\gamma_1$34.5 Protein Interacts with ICP0 and Blocks Its Ubiquitination. We hypothesized that HSV $\gamma_1$34.5 may interact with ICP0 to prevent its degradation. To investigate this, we carried out immunoprecipitation analysis. When ectopically expressed in 293T cells, full-length $\gamma_1$34.5 coprecipitated with ICP0 (*SI Appendix*, Fig. S6*A*). The mutant N159, which has deletion of the carboxyl-terminal domain of $\gamma_1$34.5, also coprecipitated with ICP0. However, the mutant ΔN146, which has a deletion of the amino-terminal domain of $\gamma_1$34.5, failed to precipitate with ICP0. These results were recapitulated in reciprocal immunoprecipitation (*SI Appendix*, Fig. S6*B*), indicating that $\gamma_1$34.5 interacts with ICP0 via its amino-terminal domain. We next verified the $\gamma_1$34.5–ICP0 interaction in virus-infected cells (Fig. 3*B*). In cells infected with wild-type HSV-1, ICP0 coprecipitated with $\gamma_1$34.5. ICP0 binding was not detectable in cells infected with R3616 or with recombinant H1001 that lacks the N-terminal domain of $\gamma_1$34.5. However, the $\gamma_1$34.5–ICP0 interaction was restored in cells infected with H1002, which bears the repaired N-terminal domain of $\gamma_1$34.5.

To further investigate the impact of the $\gamma_1$34.5–ICP0 interaction, we measured ICP0 expression in virus-infected cells. The steady-state levels of ICP0 were sharply reduced in R3616-infected cells relative to cells infected with wild-type HSV-1 (Fig. 3*C*). Similarly, a reduction in ICP0 protein levels was seen with recombinant H1001 but not with H1002. This was not due to the differences in viral infectivity as the expression of ICP4 and ICP27 were comparable. Moreover, treatment of cells with MG132 restored ICP0 expression to an appreciable level (Fig. 3*C*). We further recapitulated these phenotypes in human lung fibroblasts (*SI Appendix*, Fig. S6*C*), suggesting that the N-terminal domain of $\gamma_1$34.5 interacts with ICP0, leading to ICP0 stabilization.

As proteasomal degradation typically involves substrate polyubiquitination, we inquired whether the $\gamma_1$34.5 protein affects ICP0 ubiquitination. We examined total ubiquitination of ICP0 in virus-infected cells, which were treated with MG312 (Fig. 3*D*). We observed that ICP0 ubiquitination was barely visible for wild-type HSV-1. However, ICP0 became heavily ubiquitinated in cells infected with R3616. This also occurred in cells infected with H1001 but not with H1002, suggesting a negative regulation of ICP0 ubiquitination by $\gamma_1$34.5 via its N-terminal domain. Consistently, unlike wild-type virus, R3616 or H1001 replicated less efficiently in MEF cells (Fig. 3*E*), which was also seen in infected human lung fibroblasts (*SI Appendix*, Fig. S6*D*). Thus, HSV-1 $\gamma_1$34.5 interacts with ICP0 through its N-terminal domain, which precludes ICP0 ubiquitination and subsequent degradation.

TRIM23 Facilitates Ubiquitination and Proteasomal Degradation of ICP0. Recent work established that TRIM23 inhibits the replication of several RNA as well as DNA viruses, including HSV-1, which relies on the activation of autophagy (33). Because TRIM23 is an E3 ubiquitin ligase that can mediate the polyubiquitination of distinct target proteins (33, 35–38), we asked whether TRIM23 contributes to the degradation of ICP0. In TRIM23$^{+/+}$ MEF cells infected with wild-type HSV-1, R3616, H1001, or H1002, the expression of ICP4 and ICP27 was similar (Fig. 4*A*). However, ICP0 expression was drastically decreased in MEFs infected with R3616 and H1001, as compared to cells infected with wild-type HSV-1 and H1002, which was attributable to the lack of functional $\gamma_1$34.5. Strikingly, in TRIM23$^{-/-}$ MEF cells infected with all viruses, there was no reduction in ICP0 expression. We verified these results by IF analysis of ICP0 and ICP27 in TRIM23$^{+/+}$ and TRIM23$^{-/-}$ cells (Fig. 4*B* and *SI Appendix*, Fig. S7 *A–D*). Furthermore, we assessed the relevance of TRIM23 in regulating ICP0 expression in human lung fibroblasts by short hairpin RNA (shRNA) knockdown analysis (*SI Appendix*, Fig. S8 *A* and *B*). Upon infection with R3616 or H1001, ICP0 expression was profoundly reduced in control cells. Depletion of TRIM23, on the other hand, robustly rescued ICP0 production. Therefore, we conclude that cellular TRIM23 triggers directly or indirectly the degradation of ICP0 during HSV infection.

To assess the importance of TRIM23 in ICP0 degradation, we examined ubiquitination of ICP0 in virus-infected cells (Fig. 4*C*). In TRIM23$^{+/+}$ cells, infection with R3616 or H1001 sharply induced the ubiquitination of ICP0, whereas infection with wild-type virus did not. H1002 behaved like wild-type HSV-1. In TRIM23$^{-/-}$ cells, HSV-1 infection failed to cause polyubiquitination of ICP0 irrespective of the status of $\gamma_1$34.5. Further analysis showed that endogenous TRIM23 coprecipitated with ICP0 in TRIM23$^{+/+}$ cells infected with R3616 or H1001 (Fig. 4*D*). Moreover, wild-type $\gamma_1$34.5 coprecipitated with ICP0 and TRIM23 upon virus infection (Fig. 4*D*). This also occurred in 293T cells ectopically expressing $\gamma_1$34.5, ICP0, and TRIM23 (*SI Appendix*, Fig. S9*A*). Notably, recombinant human TRIM23 bound to purified $\gamma_1$34.5 and ICP0 (*SI Appendix*, Fig. S9 *B* and *C*), demonstrating direct protein–protein interactions. These results suggest that $\gamma_1$34.5, ICP0, and TRIM23 can directly form a complex in HSV-1-infected cells. In the absence of functional $\gamma_1$34.5, HSV-1 infection triggers TRIM23 activation and subsequent ICP0 ubiquitination.

We next examined the role of TRIM23 in the restriction of wild-type HSV-1 and $\gamma_1$34.5 mutant viruses. Congruently, in TRIM23$^{+/+}$ cells, wild-type HSV-1 as well as H1002 grew robustly, whereas R3616 and H1001 replicated poorly, with a >100-fold decrease in viral production (Fig. 4*E*). In TRIM23$^{-/-}$ cells, the viral replication defect associated with R3616 or H1001 was rescued significantly (>100-fold increase of replication). We also found similar phenotypes in human lung fibroblasts (*SI Appendix*, Fig. S8*C*). Together, these data show that the interaction of TRIM23 and $\gamma_1$34.5 regulates ICP0 expression and subsequent viral replication.

The $\gamma_1$34.5 Protein Inhibits K11/K48-Linked Ubiquitination of ICP0. To delineate the mechanism of ICP0 degradation, we assessed the relation of TRIM23, ICP0, and $\gamma_1$34.5. As TRIM23 bound to ICP0 (Fig. 5*A*), we asked whether TRIM23 is able to directly mediate ubiquitination of ICP0. After cotransfection of wild-type ubiquitin and ICP0 into 293T cells, TRIM23 expression readily induced ICP0 ubiquitination (Fig. 5*B*), which was undetectable in the absence of TRIM23 (*SI Appendix*, Fig. S10*A*). Biochemical analysis of cells expressing TRIM23 together with different ubiquitin mutants in which specific lysines were substituted (Fig. 5*B*) showed only K11 but not K6, K27, K29, K33, K48, or K63 linked ubiquitination for ICP0. Moreover, K11R substitution in ubiquitin abolished ICP0 ubiquitination (Fig. 5*C*), indicative of K11-linked ubiquitination of ICP0 induced by TRIM23. This paralleled with K27/29-linked autoubiquitination of TRIM23 (*SI Appendix*, Fig. S10*B*), suggesting an involvement of active TRIM23 to mediate ICP0 ubiquitination (33). Deletion of N-terminal RING, C-terminal ARF, or both domains in TRIM23 abolished its capacity to ubiquitinate ICP0 (*SI Appendix*, Fig. S10 *C* and *D*). Furthermore, C34A substitution in the RING domain or K458I substitution in the ARF domain abolished K11-linked ubiquitination of ICP0 as these mutations inhibit TRIM23's enzymatic activities (33). These results suggest that TRIM23 interacts with viral ICP0 and mediates K11-linked ubiquitination through its E3 ligase activity.

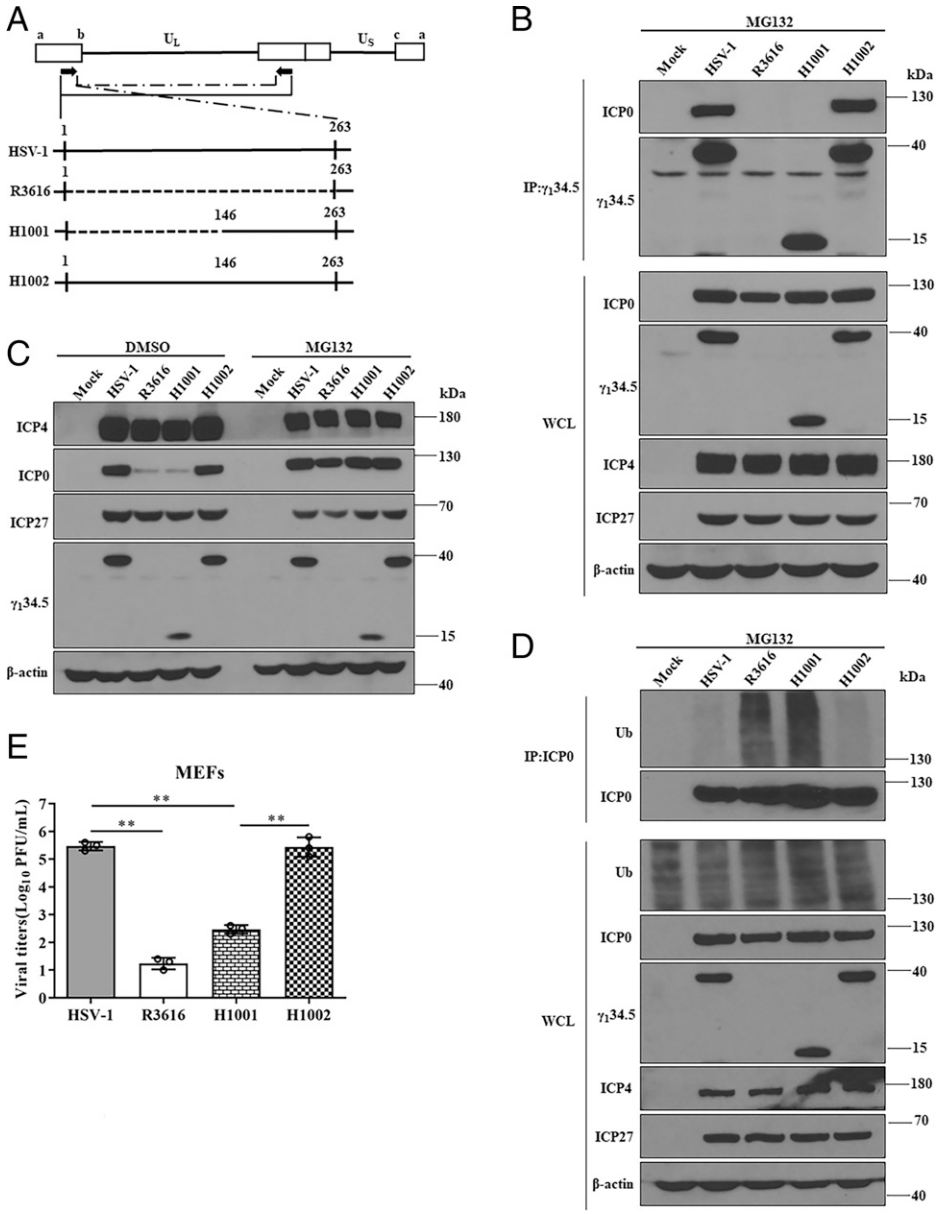

Fig. 3. The amino-terminal domain of $\gamma_1$34.5 interacts with and stabilizes ICP0. (*A*) Schematic representation of the genome structure of wild-type HSV-1 and related mutants. Two copies of $\gamma_1$34.5 loci were in repeated regions. HSV-1 is wild-type virus, whereas R3616 lacks the entire $\gamma_1$34.5 coding region. H1001 has deletion of amino acids 1 through 146 of $\gamma_1$34.5, and H1002 is a repair virus of H1001 that harbors wild-type $\gamma_1$34.5. (*B*) The amino-terminal domain of $\gamma_1$34.5 interacts with ICP0 in virus infection. MEFs were infected with the indicated viruses (MOI = 5) for 2 h and then treated with DMSO or MG132 (20 μM) for additional 6 h. Cells were processed for immunoprecipitation (IP) with anti-$\gamma_1$34.5 antibody. Whole-cell lysates (WCL) and precipitated proteins were probed with antibodies against ICP0, $\gamma_1$34.5, ICP4, ICP27, and β-actin. (*C*) Effect of $\gamma_1$34.5 mutants on the IE proteins ICP4, ICP0, and ICP27. MEFs were mock infected or infected as in *B* and harvested for Western blot analysis with antibodies against ICP4, ICP0, ICP27, $\gamma_1$34.5, and β-actin. (*D*) Effect of $\gamma_1$34.5 mutants on ICP0 ubiquitination. MEFs were mock infected or infected with the indicated viruses for 2 h (MOI = 5) and then treated with MG132 (20 μM) for additional 6 h. Cells were processed for IP with anti-ICP0 antibody. WCLs and precipitated proteins were probed with antibodies against Ub, ICP0, $\gamma_1$34.5, ICP4, ICP27, and β-actin. (*E*) Viral replication on MEFs. Cells were infected with the indicated viruses (MOI = 0.01) for 48 h, and the total virus yields were titrated by plaque assay on Vero cells. Data are expressed as means ± SD (n = 3) in *E*, $^{**}P < 0.01$ (one-way ANOVA). The data are representative of results from three (*C* and *E*) or two (*B* and *D*) independent experiments.

Next, we tested the effect of $\gamma_1$34.5 on ICP0 ubiquitination by TRIM23 (Fig. 5*D*). Unlike the vector control, wild-type $\gamma_1$34.5 prevented K11-linked ICP0 ubiquitination by TRIM23 when coexpressed. Coexpression of $\gamma_1$34.5 N159 that lacks the C-terminal domain also exhibited an inhibitory activity on ICP0 ubiquitination, while expression of ΔN146 devoid of the N-terminal domain of $\gamma_1$34.5 had no effect. As TRIM23 activation requires K27-linked autoubiquitination (33), we further assessed the effect of $\gamma_1$34.5 on this activity in 293T cells (Fig. 5*E*). We noted that wild-type $\gamma_1$34.5 inhibited the autoubiquitination of TRIM23. Moreover, N159 but not ΔN146 blocked TRIM23 autoubiquitination. These activities paralleled with the ability of $\gamma_1$34.5 variants to interact with TRIM23 as measured by immunoprecipitation (Fig. 5*F*). Mutational analysis showed that $\gamma_1$34.5 bound to the ARF domain of TRIM23, which contains the sites for autoubiquitination (*SI Appendix*, Fig. S10*E*). These results suggest that binding of $\gamma_1$34.5 to the ARF domain via its N terminus

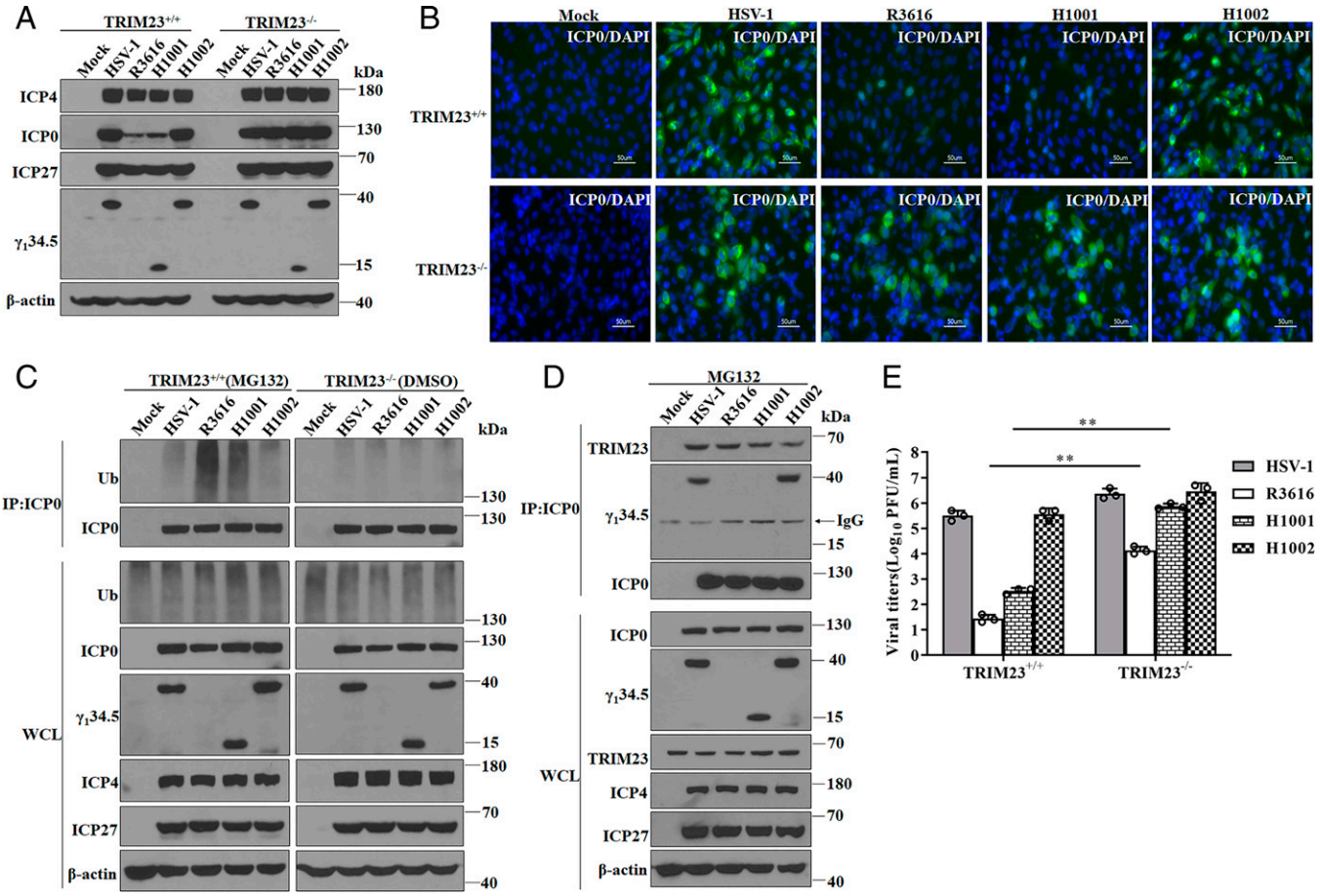

Fig. 4. TRIM23 targets ICP0 to promote its ubiquitination and degradation. (*A*) Effect of TRIM23 on the IE proteins ICP4, ICP0, and ICP27. TRIM23$^{+/+}$ and TRIM23$^{-/-}$ MEFs were mock infected or infected with the indicated viruses (MOI = 5). At 8 h postinfection, cells were harvested for Western blot determination with antibodies against ICP4, ICP0, ICP27, $\gamma_1$34.5, and β-actin. (*B*) IF analysis for ICP0. TRIM23$^{+/+}$ and TRIM23$^{-/-}$ MEFs were mock infected or infected with indicated viruses (MOI = 5) for 8 h and then stained with the ICP0 antibody (green) and DAPI (blue). (*C*) ICP0 ubiquitination in virus-infected TRIM23$^{+/+}$ and TRIM23$^{-/-}$ MEFs. Cells were mock infected or infected with indicated viruses (MOI = 5) and then treated with MG132 (20 μM) or DMSO. At 8 h post infection, lysates of cells were processed for immunoprecipitation with anti-ICP0 antibody. Whole-cell lysates (WCL) and precipitated proteins were probed with antibodies against Ub, ICP0, $\gamma_1$34.5, ICP4, ICP27, and β-actin. (*D*) TRIM23 interacts with ICP0 and $\gamma_1$34.5 in virus-infected cells. MEFs were mock infected or infected with the indicated viruses (MOI = 5) and treated with MG132 (20 μM). At 8 h post infection, lysates of cells were processed for immunoprecipitation with anti-ICP0 antibody. WCLs and precipitated proteins were probed with antibodies against ICP0, TRIM23, $\gamma_1$34.5, ICP4, ICP27, and β-actin. (*E*) Viral replication in TRIM23$^{+/+}$ and TRIM23$^{-/-}$ MEFs. Cells were infected with the indicated viruses (MOI = 0.01). At 48 h post infection, the total virus yields were titrated by plaque assay on Vero cells. Data are expressed as means ± SD (n = 3) in *E*, $^{**}P < 0.01$ (one-way ANOVA). The data are representative of results from three (*A* and *E*) or two (*C* and *D*) independent experiments. The images are representative of results from at least 10 images for *B*.

inactivates TRIM23 and prevents TRIM23-mediated, K11-linked ubiquitination of ICP0.

To validate the impact of $\gamma_1$34.5, we examined ICP0 ubiquitination in virus-infected cells. For this purpose, we established TRIM23$^{+/+}$ and TRIM23$^{-/-}$ cell lines stably expressing HA-tagged ubiquitin K11-only. As shown in Fig. 5*G*, infection with R3616 or H1001 apparently induced K11-linked ubiquitination of ICP0 in TRIM23$^{+/+}$ (HA-K11) cells. Interestingly, this was accompanied by K48-linked ubiquitination of ICP0. However, neither wild-type HSV-1 nor H1002 infection evoked ubiquitination of ICP0. Importantly, in TRIM23$^{-/-}$ (HA-K11) cells, viral infections did not cause apparent K11- or K48-linked ubiquitination in ICP0. These results suggest that in virus-infected cells, TRIM23 either directly or indirectly controls both K11- and K48-linked ubiquitination of ICP0, whereas the viral $\gamma_1$34.5 protein blocks this process to promote viral replication.

TRIM23 Limits Replication of HSV Deleted of the ICP0 Gene. ICP0 is an immediate early protein that activates the expression of early and late HSV genes, resulting in productive infection (2). Since ICP0 is targeted by TRIM23, we investigated their functional link in viral replication (Fig. 6*A*). In TRIM23$^{+/+}$ cells, wild-type HSV-1 expressed appreciable levels of mRNA for ICP4, ICP27, and gC and gD (late genes). Although R7910, a mutant virus that lacks the ICP0 gene, efficiently expressed mRNA for ICP4 and ICP27, it had a drastic reduction in gC and gD mRNA expression, indicative of defective viral replication. Recombinant R7911, which has the repaired ICP0 gene, had restored mRNA expression for gC and gD. Notably, in TRIM23$^{-/-}$cells, replication defects associated with R7910 were significantly rescued. Similar patterns of protein expression were noted for ICP4, ICP27, gC, and gD as measured by immunoblot and IF analyses (Fig. 6 *B–D* and *SI Appendix*, Fig. S11). These results suggest that TRIM23, besides its role in autophagy (33, 39), restricts HSV-1 via ICP0 degradation.

We next determined viral production by plaque assay (Fig. 6*E*). In TRIM23$^{+/+}$ cells, wild-type HSV-1 as well as R7911 grew efficiently, reaching titers of 4×10^5 and 5×10^5 pfu/mL, respectively. However, R7910 grew less efficiently, with a titer reaching 2×10^3 pfu/mL. In TRIM23$^{-/-}$ cells, HSV-1 and R7911 grew to titers of 3×10^6 pfu/mL. Remarkably, R7910 grew to a titer of 4×10^5

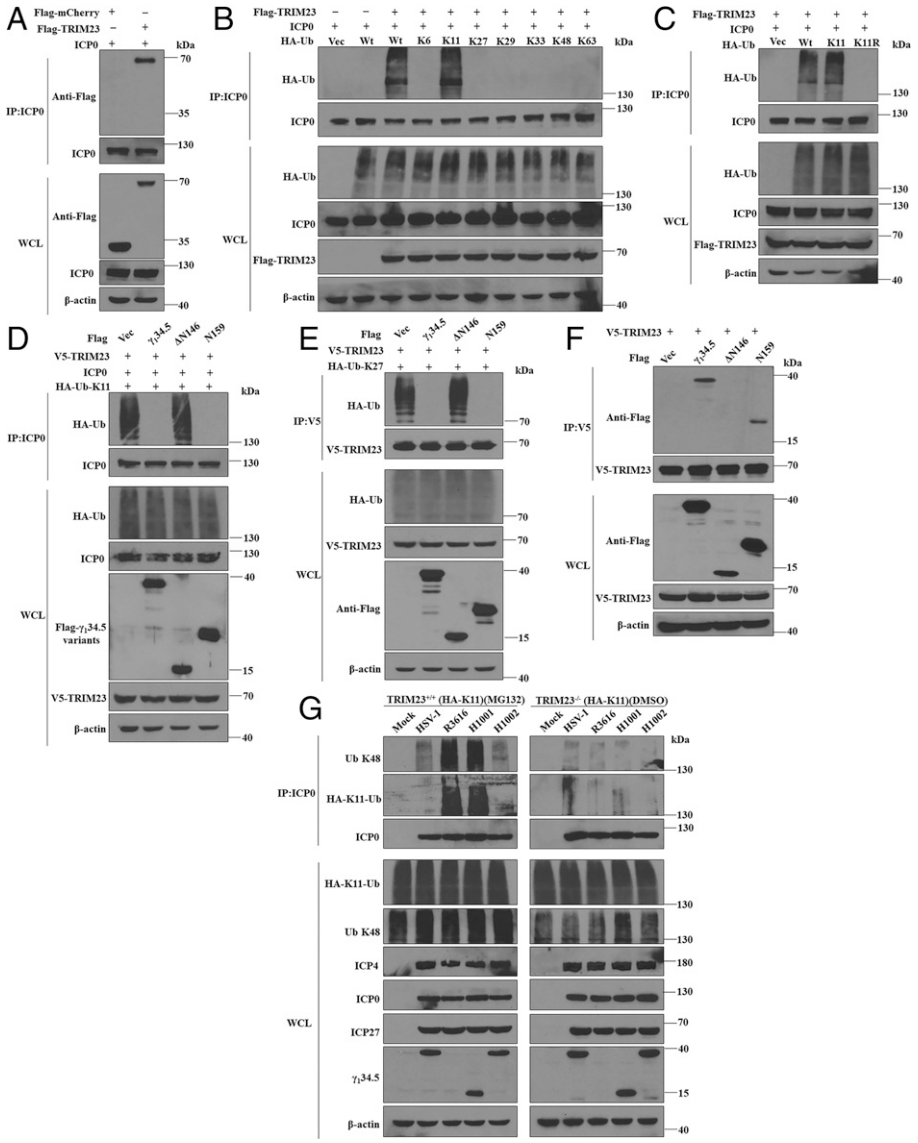

Fig. 5. The $\gamma_1$34.5 protein inhibits ubiquitination of ICP0 mediated by TRIM23. (*A*) TRIM23 interacts with ICP0. HEK-293T cells were transiently transfected with pcDNA-ICP0, Flag-mCherry, or Flag-TRIM23 and then harvested for immunoprecipitation with anti-ICP0 antibody and Western blot analysis. (*B*) TRIM23 mediates K11-linked ubiquitination of ICP0. Flag-TRIM23 was cotransfected with pcDNA-ICP0 along with Vector, HA-Ub (Wt), or the indicated Ub mutants into HEK-293T cells. Cells were harvested for immunoprecipitation with anti-ICP0 antibody at 48 h posttransfection. Whole-cell lysates (WCL) and precipitated proteins were probed with antibodies against ICP0, HA, Flag, and β-actin. (*C*) K11R substitution in ubiquitin abolishes ICP0 ubiquitination by TRIM23. Ubiquitination assay was done as in *B* with pcDNA-ICP0, Flag-TRIM23, Wt, HA-Ub (K11 only), and HA-Ub (K11R). (*D*) Effects of $\gamma_1$34.5 mutants on K11-linked ubiquitination of ICP0 by TRIM23. HEK-293T cells were transiently transfected pcDNA-ICP0, V5-TRIM23, and HA-Ub (K11 only) along with Flag-Vec, Flag-$\gamma_1$34.5, Flag-ΔN146, or Flag-N159. Cells were then harvested for immunoprecipitation and Western blot analysis with indicated antibodies. (*E*) Effects of $\gamma_1$34.5 variants on K27-linked autoubiquitination of TRIM23. HEK-293T cells were transfected V5-TRIM23, HA-Ub (K27 only) along with Flag-Vec, Flag-$\gamma_1$34.5, Flag-ΔN146, or Flag-N159. Cells were then harvested for immunoprecipitation and Western blot analysis with indicated antibodies. (*F*) The N terminus of $\gamma_1$34.5 interacts with TRIM23. HEK-293T cells were transfected V5-TRIM23 along with Flag-Vec, Flag-$\gamma_1$34.5, Flag-ΔN146, or Flag-N159 and assessed by immunoprecipitation and Western blot analysis with indicated antibodies. (*G*) Effects of TRIM23 and $\gamma_1$34.5 on K11- and K48-linked ubiquitination of ICP0 in virus-infected cells. TRIM23$^{+/+}$ and TRIM23$^{-/-}$ MEFs stably expressing HA-Ub (K11 only) were mock infected or infected with the indicated viruses (MOI = 5) and then treated with DMSO or MG132 (20 μM) for 6 h. Cells were processed for immunoprecipitation with anti-ICP0 antibody. WCLs and precipitated proteins were probed with antibodies against HA and Ub (K48), ICP0, $\gamma_1$34.5, ICP4, ICP27, and β-actin. All the data are representative of results from two independent experiments.

pfu/mL. This recovery was attributable to the deficiency of TRIM23. These growth patterns were also notable in human lung fibroblasts upon depletion of TRIM23 by shRNA (*SI Appendix*, Fig. S12*A*). Moreover, ectopic expression of wild-type TRIM23 in TRIM23$^{-/-}$ cells reduced replication of R7910 (Fig. 6*F*). This inhibitory effect was not seen with ectopic expression of inactive TRIM23 truncation mutants, indicating that enzymatically active TRIM23 restricts replication of the ICP0 null mutant (*SI Appendix*, Fig. S12*B*).

Discussion

Productive herpesvirus infection relies on immediate early proteins that drive viral replication (1, 2). Prior work showed that host microRNA-138 represses mRNA expression of ICP0, which facilitates HSV-1 latency (40). The identification of $\gamma_1$34.5 as a positive regulator of ICP0 expression highlights complex mechanisms in HSV biology. This may seem unexpected as $\gamma_1$34.5 is classically categorized as a leaky late (γ_1) gene product (41). However, we and others showed that the

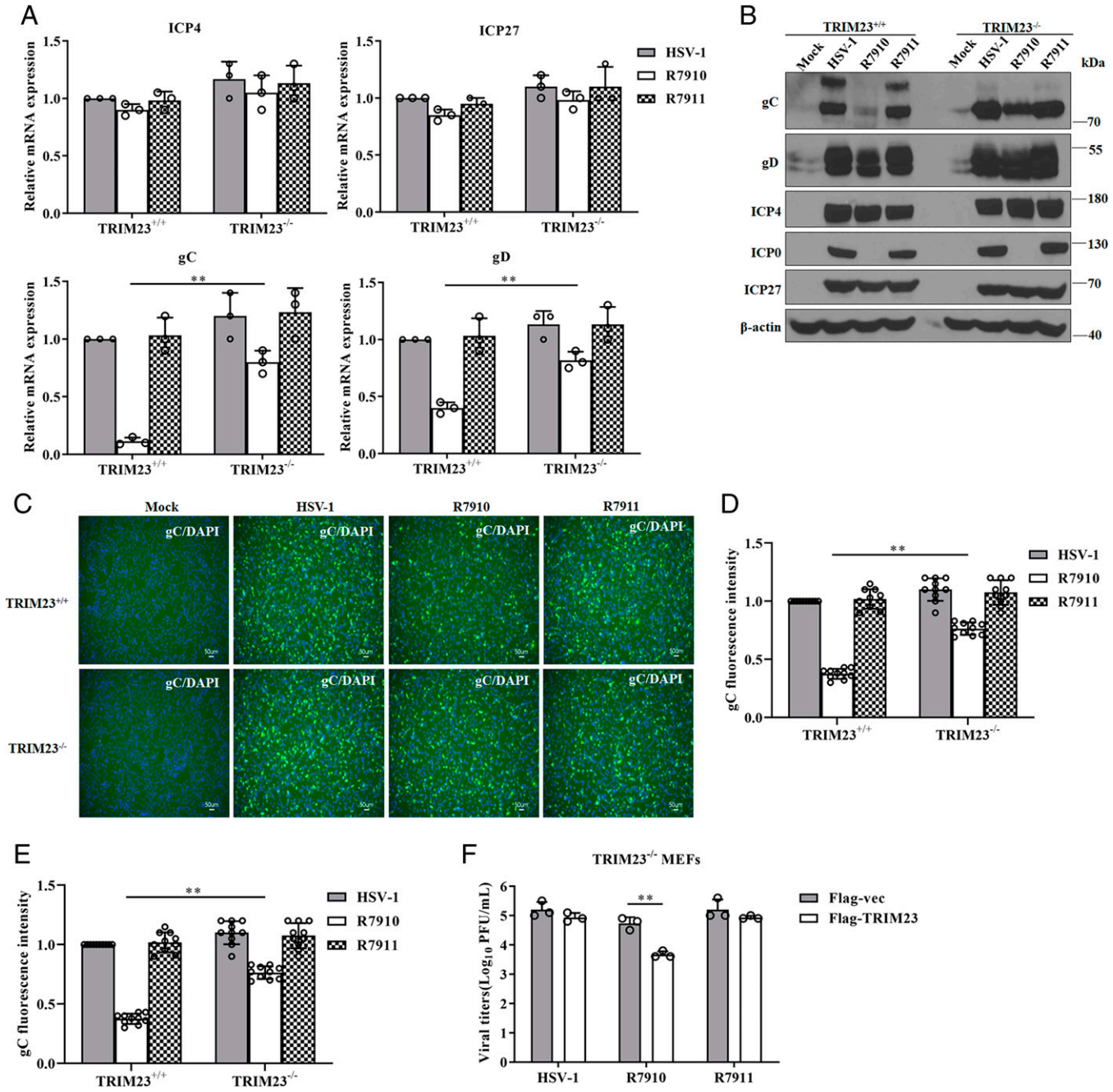

Fig. 6. TRIM23 inhibits replication of HSV deficient in ICP0. (*A*) Viral mRNA expression analysis. TRIM23$^{+/+}$ and TRIM23$^{-/-}$ MEFs were infected with the indicated viruses (HSV-1, R7910, or R7911) at an MOI of 5 for 12 h and harvested for qRT-PCR analysis of ICP4, ICP27, gC, and gD. (*B*) Viral protein production in TRIM23$^{+/+}$ and TRIM23$^{-/-}$ MEFs that were mock infected or infected as in *A* at 12 h post infection. Cells were harvested for Western blot analysis with antibodies against ICP4, ICP0, ICP27, gC, gD, and β-actin. (*C*) IF analysis of gC in TRIM23$^{+/+}$ and TRIM23$^{-/-}$ MEFs that were mock infected or infected viruses as in *A* and then stained with gC antibody (green) and DAPI (blue). (*D*) Quantification of gC. IF images in *C* were quantified using NIH ImageJ software (set the HSV-1 in TRIM23$^{+/+}$ group as 1.0). (*E*) Viral replication in TRIM23$^{+/+}$ and TRIM23$^{-/-}$ MEFs that were infected with the indicated viruses (MOI = 0.01). At 48 h postinfection, viral yields were titrated by plaque assay on U2OS cells. (*F*) Effect of TRIM23 on viral replication. TRIM23 in TRIM23$^{-/-}$ cells were transiently transfected with Flag-Vec or Flag-TRIM23 for 24 h. Cells were then infected with HSV-1, R7910, or R7911 (MOI = 0.01). Viral yields were determined by plaque assay on U2OS cells at 48 h postinfection. One-way ANOVA was used for *A*, *D*, *E*, and *F*, $^{**}P < 0.01$. Data are expressed as means ± SD ($n = 3$) in *A*, *E*, and *F* and quantified from at least an average 10 images per group in *D*. The data shown in *A*, *B*, *E*, and *F* are representative of results from three independent experiments. The images are representative of results from at least 10 images for *C*.

$\gamma_1$34.5 protein is expressed in both early and later stages of HSV infection (10, 42). Numerous studies indicated that the immediate early protein ICP0 critically regulates epigenetic modification, interferon expression, the DNA damage response, and autophagy (2, 3, 43). Notably, mutations in ICP0 attenuate HSV-1 and impair viral reactivation (44–48). We infer that a wide window of $\gamma_1$34.5 expression may have coopted to stabilize ICP0 in the face of host restriction. In line with this, wild-type virus but not the $\gamma_1$34.5 null mutant retained steady-state ICP0 expression independently of TBK1 or Us11. A similar phenotype for ICP0 expression was reported by others, and PKR pathway activation was hypothesized to play a role (49).

We recently reported that ICP0 accumulation is separable from eIF2α phosphorylation (50), suggesting that a distinct mechanism exists. Our data establish a functional relationship between $\gamma_1$34.5 and ICP0, which may partly explain why deletion of $\gamma_1$34.5 renders HSV avirulent and cripples viral reactivation from latency (20, 21, 23). Perhaps the $\gamma_1$34.5–TRIM23–ICP0 axis acts as a switch in this context, which may confer an advantage to HSV persistency.

The $\gamma_1$34.5 protein binds to the TRIM23–ICP0 complex, which prevents the K11- and K48-linked ubiquitination and degradation of ICP0 in virus-infected cells. This is attributable to functional interference rather than disruption of the TRIM23–ICP0 interaction. We noted that the $\gamma_1$34.5 protein bound to the ARF domain of TRIM23, which inhibited the K27-linked autoubiquitination of TRIM23. Moreover, the $\gamma_1$34.5 protein bound to ICP0 and prevented its K11-linked ubiquitination by TRIM23. These activities involved the amino-terminal domain of $\gamma_1$34.5, which is predicted to form four α-helices separated by a stretch of turn or coil regions. Given a direct interaction of $\gamma_1$34.5 and TRIM23, a plausible mechanism would be that one or more of these α-helices may directly interfere with TRIM23 activity. In addition, these modules may create physical hindrance to shield ICP0. These models are not mutually exclusive and should be investigated in future studies.

TRIM family proteins play a diverse role in viral infection (24, 25). Of note, TRIM23 activates autophagy to inhibit the replication of certain RNA viruses and DNA viruses, including HSV-1 (33). In doing so, TRIM23 undergoes K27-linked autoubiquitination at the ARF domain to activate its ARF GTPase, which recruits TBK1 to autophagosomes and facilitates phosphorylation of the autophagy receptor p62. TRIM23 is also reported to regulate interferon responses both positively and negatively during certain RNA virus infections (36, 37). Our data reveal that TRIM23 directly interacts with and drives ICP0 for proteasomal degradation. Importantly, depletion of TRIM23 markedly rescues HSV-1 replication. These results underscore the importance of TRIM23 in HSV-1 restriction, although the mechanism of TRIM23 activation during HSV-1 infection awaits investigation. In addition, other TRIM family members also interplay with ICP0. For example, TRIM22 inhibits ICP0 expression by epigenetic repression (32). Conversely, ICP0 mediates degradation of cellular TRIM27 by functioning as a viral E3 ligase (51). Given that TRIM23 activates autophagy and also facilitates proteasomal degradation of ICP0, we speculate that this dual mechanism may proceed concurrently or temporally to control HSV infection.

TRIM23 is a unique E3 ubiquitin ligase that harbors in addition to its RING E3 ligase domain, also a GTPase in the C-terminal ARF domain (33, 35). We show that proteasomal degradation of ICP0 by TRIM23 is coupled with both K11- and K48-linked ICP0 polyubiquitination in virus-infected cells. Genetic deletion of TRIM23 abolishes the observed activities. Intriguingly, TRIM23 selectively catalyzes K11-linked ubiquitination of ICP0 when ectopically expressed. This involves active TRIM23 that is capable of undergoing K27-linked autoubiquitination. Although incompletely deciphered, we suspect that upon virus infection, a distinct E3 ligase may catalyze K48-linked polyubiquitination of ICP0 following its K11-linked ubiquitination by TRIM23. Alternatively, an additional factor that is at a limiting rate in our experiments may cooperate with TRIM23 to catalyze K48-linked ubiquitination. As such, by selectively regulating ICP0 ubiquitination in virus infection, TRIM23 may limit HSV gene expression and subsequent replication.

In summary, this work shows that both HSV $\gamma_1$34.5 and TRIM23 control ICP0 expression but in opposite ways. TRIM23 functions to induce proteasomal degradation of ICP0 in virus-infected cells. On the other hand, viral $\gamma_1$34.5 stabilizes ICP0 by engaging with the TRIM23–ICP0 complex. These results unveil a previously unrecognized posttranslational regulatory circuit in HSV infection. Our findings suggest that modulation of TRIM23 and $\gamma_1$34.5 may be a promising approach to block HSV lytic replication or reactivation.

Methods

Cells and Viruses. MEF, Vero, U2OS, human embryonic kidney (HEK)-293T, and human lung embryonic (HEL) fibroblast cells were obtained from the American Type Culture Collection. TRIM23$^{+/+}$, TRIM23$^{-/-}$, TBK1$^{+/+}$, and TBK1$^{-/-}$ MEFs, HEL stably expressed non-target shRNA, and TRIM23 target shRNA were previously described (10, 39, 52). TRIM23$^{+/+}$ or TRIM23$^{-/-}$ MEFs stably expressing HA-Ub (K11 only) were selected with puromycin (Santa Cruz Biotechnology) at the concentration 3 μg/mL. All cells were grown in Dulbecco's modified Eagle's medium (Gibco) containing 10% or 5% fetal bovine serum (Gibco) in a humidified 5% CO_2 incubator at 37 °C.

HSV-1(F) is a prototype HSV-1 strain used in this study (53). In recombinant virus R3616, a 1-kb fragment from the coding region of the $\gamma_1$34.5 gene was deleted (18). In recombinant virus H1001, the region encoding amino acids 1 through 146 of $\gamma_1$34.5 was deleted (54), and in H1002, the deleted region was repaired with wild-type $\gamma_1$34.5 (54). Recombinant virus R7910, lacking both copies of the ICP0, was described elsewhere (55). In recombinant virus R7911, the deleted ICP0 gene was restored (56). R3631 is deleted from the Us11 gene (57). Preparation of viral stock and titration of infectivity were carried out in Vero and U2OS cells.

Plasmids and Transfection. pCMV6-TRIM23-MYC-DDK (Flag-TRIM23), purchased from OriGene (NM_033227), was used as a PCR template to generate the truncation mutants, which were inserted into the *Sgf*I and *Mlu*I sites the pCMV6-MYC-DDK vector. Specifically, ΔRING expresses amino acids 88 through 574, ΔARF contains amino acids 1 through 402, CENTRAL encodes amino acids 88 through 402, RING carries amino acids 1 through 88, and ARF expresses amino acids 403 through 574. Point mutants C34A and K458I in pCMV6-TRIM23-MYC-DDK were previously described (33). Plasmid complementary DNA (pcDNA)-ICP0 were obtained by inserting ICP0 complementary DNA (cDNA) into the HindIII and BamHI sites of pcDNA 3.1. V5-TRIM23, HA-$\gamma_1$34.5, Flag-$\gamma_1$345, Flag-ΔN146 (deleted 1 through 146 aa of $\gamma_1$34.5), and Flag-N159 (contained 1 through 159 aa of $\gamma_1$34.5) were previously described (10, 54, 58). HA-Ub (wild type [WT]) (#17608) and the mutants HA-Ub (K6 only) (#22900), HA-Ub (K11 only) (#22901), HA-Ub (K27 only) (#22902), HA-Ub (K29 only) (#22903), HA-Ub (K33 only) (#17607), HA-Ub (K48 only) (#17605), and HA-Ub (K63 only) (#17606) were from Addgene. HA-Ub (K11R) was generated by site-directed mutagenesis with QuikChange II Site-Directed Mutagenesis Kit (Agilent Technologies) using the HA-Ub (WT) as the template. pCDH-HA-Ub (K11 only) was obtained by inserting HA-Ub (K11 only) into the *BamH*I and *Not*I sites of pCDH-EF1-MCS-T2A-Puro (#CD527A-1, SBI System Biosciences). Lentivirus package plasmids (pCMV-VSV-G, pMDLg/pRRE, and pRSV-REV) were previously described (59). All plasmids or constructs were produced from *Escherichia coli* strain Top10 (Thermo Fisher Scientific). New constructs were sequenced by Research Resources Center in University of Illinois Chicago. The primers used for plasmids construction were listed in *SI Appendix*, Table S1. Plasmid transfection was done with Lipofectamine LTX or PLUS (Thermo Fisher Scientific) according to the manufacturer's instruction.

Antibodies. For immunoblot analysis, the following antibodies were used: α-ICP4 (1:1,000, H943, Santa Cruz Biotechnology), α-ICP0 (1:1,000, 11060, Santa Cruz Biotechnology), α-ICP27 (1:4,000, H1113, Virusys), α-$\gamma_1$34.5 (1:4,000 (60), α-gC (1:4,000, 3G9, Abcam), α-gD (1:1,000, DL6, Santa Cruz Biotechnology), α-β-actin (1:2,000, AC-15, Sigma), α-ubiquitin (horseradish peroxidase [HRP] Conjugate) (1:1,000, P4D1, Cell signaling technology), α-K48-ubiquitin (1:1,000, D9D5, Cell Signaling technology), α-TRIM23 (1:3,000, EPR7787, Abcam), α-FLAG (HRP Conjugate) (1:2,000, M2, Sigma-Aldrich), α-HA (HRP Conjugate) (1:1,000, 6E2, Cell Signaling technology), α-V5 (1:1,000, H-9, Santa Cruz Biotechnology), α-TRIM23 (1:1,000, C-1, Santa Cruz Biotechnology), α-rabbit IgG-HRP (1:10,000, Santa Cruz Biotechnology), and α-mouse IgG-HRP (1:10,000, Santa Cruz Biotechnology). For IF staining, the following antibodies were used: α-ICP0 (1:100, 11060, Santa Cruz Biotechnology), α-ICP27 (1:100, H1113, Santa Cruz Biotechnology), α-ICP4 (1:100, DL6, Santa Cruz Biotechnology), α-gC (1:500, 3G9, Abcam), DAPI (1:1,000, Sigma-Aldrich), and α-Mouse IgG (H+L)-Alexa Fluor 488 (1: 1000, Thermo Fisher Scientific).

Viral Infections. Cells were infected with viruses at appropriate multiplicities of infection (MOI). Viral titers were determined by plaque assay on Vero or U2OS cells (10). To assay for protein degradation, cells were infected with viruses at an MOI of 5. At 2 h postinfection, cells were untreated or treated

with lactacystin (20 μM, Santa Cruz Biotechnology), MG132 (20 μM, Sigma-Aldrich), z-VAD-FMK (50 μM, Santa Cruz Biotechnology), 3-methyladenine (5 mM, Sigma-Aldrich), chloroquine (10 μM, Sigma-Aldrich), and bafilomycin A1 (20 nM, Santa Cruz Biotechnology) for 6 h, respectively. Cells were harvested for Western blot, immunoprecipitation, or ubiquitination analysis.

Real-Time qPCR Assay. Total RNA was harvested from cells using an RNeasy Plus mini kit (Qiagen) according to the manufacturer's instruction, and the genomic DNA was eliminated using genomic DNA Eliminator columns. Aliquots of RNA (~200 ng) were used for cDNA synthesis with a high-capacity cDNA reverse transcription kit with RNase inhibitor (Applied Biosystems). Real-time qPCR was performed on Applied Biosystems ABI Prism 7900HT instrument with SYBR green master mix (Applied Biosystems). Gene expression levels were normalized to that of endogenous control 18S ribosomal RNA. Relative gene expression was determined as described previously (54, 61). The comparative cycle threshold (CT) method (ΔΔCT) was used to measure the induction of each target gene relative to its induction in mock-infected cells. Primer sequences were listed in *SI Appendix*, Table S1.

IF Assay. Cells were cultured on coverslips to 90% confluency and infected with indicated viruses for 8 h with or without MG132 (20 μM, Sigma-Aldrich). Cells were then fixed with 4% paraformaldehyde in phosphate-buffered saline (PBS) for 15 min at room temperature. After permeabilization with 0.1% Triton X-100 in PBS for 10 min, cells were blocked with 3% bovine serum albumin (BSA) in PBS for 1 h and incubated with primary antibodies overnight at 4 °C. This was followed by incubation with a fluorescein-conjugated secondary antibody for 1 h. After washing with PBS, cells were mounted, and images were acquired under a Keyence fluorescence microscope. The median fluorescence intensity was quantified as the total fluorescence intensity divided by the total number of nuclei which was normalized to DAPI staining. All image quantifications were performed using cell counting software in Keyence fluorescence microscope and ImageJ, the ImageJ distribution, Fiji (62, 63).

Western Blot. Cells were harvested, washed with PBS, and then lysed on ice for 30 min as described previously (54). Lysates of cells were subjected to electrophoresis on 8%, 10%, or 12% Bis-Tris sodium dodecyl sulfate–polyacrylamide gel electrophoresis (SDS-PAGE) gels (pH 6.4). Proteins were transferred to polyvinylidene difluoride membranes, blocked in 3% (wt/vol) BSA in phosphate buffer saline-tween-20 (PBS-T), and incubated with the indicated primary antibodies at 4 °C overnight. After washing with PBS-T, membranes were incubated with HRP-conjugated secondary antibodies diluted in 3% (wt/vol) BSA in PBS-T for 1 h at room temperature. Proteins were visualized using SuperSignal West Pico Plus chemiluminescent reagent (Thermo Fisher Scientific) and detected by a X-ray film system (Thomas Scientific).

Protein–Protein Interaction and Ubiquitination Assays. Immunoprecipitation was performed as described previously (54). Briefly, cells were lysed in Nonidet P-40 (Nonidet P-40) buffer (50 mM Tris·HCl (pH 7.4), 1% Nonidet P-40, 150 mM NaCl, 1 mM EDTA, 1:400 protease inhibitor mixture), and then centrifuged at 20,000 × g for 10 min at 4 °C. An aliquot of whole-cell lysates was saved for immunoblot analysis. The rest were incubated with the indicated antibodies overnight followed by agarose conjugated with protein A/G (sc-2003, Santa Cruz Biotechnology) for 4 h. The beads were washed three times with wash buffer (50 mm Tris·HCl, pH 7.4, 150 mm NaCl, 5 mm EDTA, 0.1% Triton X-100, and protease inhibitor mixture). The precipitated proteins were subjected to Western blot analysis using the indicated antibodies. For detection of ICP0 or TRIM23 ubiquitination, cells were lysed with lysis buffer (1% SDS, 150 mM NaCl, and 10 mM Tris·HCl, pH 8.0) with 2 mM sodium orthovanadate, 50 mM sodium fluoride, and protease inhibitors. Samples were processed as for immunoprecipitation but washed with radio immunoprecipitation assay buffer containing 2 M urea to remove nonspecific binding of other ubiquitinated proteins.

For in vitro binding assays, FLAG-tagged $\gamma_1$34.5 protein, expressed in HEK-293T cells, was purified using anti-FLAG-conjugated magnetic beads (M2, Sigma-Aldrich). FLAG-$\gamma_1$34.5 immobilized on beads or control beads were incubated with recombinant human GST-TRIM23 protein (Abnova, H00000373-P01) in PBS (final concentration of 5 μg/mL) for 8 h at 4 °C. After extensive washing with 1% Nonidet P-40 buffer, bound proteins were eluted from the beads in Laemmli buffer by heating at 95 °C for 5 min and then subjected to SDS-PAGE and immunoblot analysis. Similarly, ICP0 was purified from transiently transfected HEK-293T cells using magnetic beads (M2, Sigma-Aldrich) and an anti-ICP0 antibody (Santa Cruz, 5H7) and tested for binding to recombinant human GST-TRIM23 (Abnova, H00000373-P01).

Lentiviral Transduction and Cell Line Construction. For construction of stably expressed HA-Ub (K11 only) in TRIM23$^{+/+}$ and TRIM23$^{-/-}$ MEFs, lentivirus was produced after transfection of pCDH-HA-Ub (K11 only) together with package plasmids (pCMV-VSV-G, pMDLg/pRRE, and pRSV-REV) in HEK-293T cells (59). TRIM23$^{+/+}$ and TRIM23$^{-/-}$ MEFs were then infected with the lentivirus. At 16 h after infection, cells were overlaid with fresh medium. At 3 d after infection, the cells were selected by 3 μg/mL puromycin (Santa Cruz Biotechnology). All experiments were performed within 2 wk after lentiviral transduction.

Statistical Analysis. All data were presented as means ± SD and analyzed using GraphPad Prism 7.0 software (GraphPad Software, Inc.). One-way ANOVA with Dunnett's multiple comparisons or an unpaired two-tailed Student's *t* test was used as indicated in the legends. The *P* values were calculated from three biological replicates unless otherwise indicated in the legends. Data were reproduced in independent experiments as indicated in the figure legends.

Data Availability. All study data are included in the article and/or *SI Appendix*.

ACKNOWLEDGMENTS. This work was supported by grants from the National Institute of Allergy and Infectious Diseases (AI148148 to B.H.) and (AI148534 and AI087846 to M.U.G.). We thank Dr. Bernard Roizman and Haidong Gu for valuable reagents.

1. R. J. Whitley, B. Roizman, Herpes simplex virus infections. *Lancet* **357**, 1513–1518 (2001).
2. D. M. Knipe, A. Cliffe, Chromatin control of herpes simplex virus lytic and latent infection. *Nat. Rev. Microbiol.* **6**, 211–221 (2008).
3. C. Boutell, R. D. Everett, Regulation of alphaherpesvirus infections by the ICP0 family of proteins. *J. Gen. Virol.* **94**, 465–481 (2013).
4. M. C. Rodríguez, J. M. Dybas, J. Hughes, M. D. Weitzman, C. Boutell, The HSV-1 ubiquitin ligase ICP0: Modifying the cellular proteome to promote infection. *Virus Res.* **285**, 198015 (2020).
5. J. Chou, B. Roizman, The $\gamma_1$34.5 gene of herpes simplex virus 1 precludes neuroblastoma cells from triggering total shutoff of protein synthesis characteristic of programed cell death in neuronal cells. *Proc. Natl. Acad. Sci. U.S.A.* **89**, 3266–3270 (1992).
6. J. Chou, B. Roizman, Herpes simplex virus 1 $\gamma_1$34.5 gene function, which blocks the host response to infection, maps in the homologous domain of the genes expressed during growth arrest and DNA damage. *Proc. Natl. Acad. Sci. U.S.A.* **91**, 5247–5251 (1994).
7. J. Chou, J. J. Chen, M. Gross, B. Roizman, Association of a M(r) 90,000 phosphoprotein with protein kinase PKR in cells exhibiting enhanced phosphorylation of translation initiation factor eIF-2 alpha and premature shutoff of protein synthesis after infection with $\gamma_1$34.5- mutants of herpes simplex virus 1. *Proc. Natl. Acad. Sci. U.S.A.* **92**, 10516–10520 (1995).
8. B. He, M. Gross, B. Roizman, The $\gamma_1$34.5 protein of herpes simplex virus 1 complexes with protein phosphatase 1alpha to dephosphorylate the alpha subunit of the eukaryotic translation initiation factor 2 and preclude the shutoff of protein synthesis by double-stranded RNA-activated protein kinase. *Proc. Natl. Acad. Sci. U.S.A.* **94**, 843–848 (1997).
9. B. He, M. Gross, B. Roizman, The $\gamma_1$34.5 protein of herpes simplex virus 1 has the structural and functional attributes of a protein phosphatase 1 regulatory subunit and is present in a high molecular weight complex with the enzyme in infected cells. *J. Biol. Chem.* **273**, 20737–20743 (1998).
10. D. Verpooten, Y. Ma, S. Hou, Z. Yan, B. He, Control of TANK-binding kinase 1-mediated signaling by the $\gamma_1$34.5 protein of herpes simplex virus 1. *J. Biol. Chem.* **284**, 1097–1105 (2009).
11. H. Jin, Z. Yan, Y. Ma, Y. Cao, B. He, A herpesvirus virulence factor inhibits dendritic cell maturation through protein phosphatase 1 and Ikappa B kinase. *J. Virol.* **85**, 3397–3407 (2011).
12. S. Pan, X. Liu, Y. Ma, Y. Cao, B. He, Herpes simplex virus 1 $\gamma_1$34.5 protein inhibits STING activation that restricts viral replication. *J. Virol.* **92**, (2018), e01015–18.
13. A. Orvedahl *et al.*, HSV-1 ICP34.5 confers neurovirulence by targeting the Beclin 1 autophagy protein. *Cell Host Microbe* **1**, 23–35 (2007).
14. S. M. Brown, A. R. MacLean, J. D. Aitken, J. Harland, ICP34.5 influences herpes simplex virus type 1 maturation and egress from infected cells in vitro. *J. Gen. Virol.* **75**, 3679–3686 (1994).
15. X. Jing, M. Cerveny, K. Yang, B. He, Replication of herpes simplex virus 1 depends on the $\gamma_1$34.5 functions that facilitate virus response to interferon and egress in the different stages of productive infection. *J. Virol.* **78**, 7653–7666 (2004).
16. S. Wu *et al.*, Herpes simplex virus 1 induces phosphorylation and reorganization of lamin A/C through the $\gamma_1$34.5 protein that facilitates nuclear egress. *J. Virol.* **90**, 10414–10422 (2016).
17. X. Liu *et al.*, The herpesvirus accessory protein $\gamma_1$34.5 facilitates viral replication by disabling mitochondrial translocation of RIG-I. *PLoS Pathog.* **17**, e1009446 (2021).

18. J. Chou, E. R. Kern, R. J. Whitley, B. Roizman, Mapping of herpes simplex virus-1 neurovirulence to $\gamma_1$34.5, a gene nonessential for growth in culture. *Science* **250**, 1262–1266 (1990).
19. A. R. MacLean, M. ul-Fareed, L. Robertson, J. Harland, S. M. Brown, Herpes simplex virus type 1 deletion variants 1714 and 1716 pinpoint neurovirulence-related sequences in Glasgow strain 17+ between immediate early gene 1 and the 'a' sequence. *J. Gen. Virol.* **72**, 631–639 (1991).
20. R. J. Whitley, E. R. Kern, S. Chatterjee, J. Chou, B. Roizman, Replication, establishment of latency, and induced reactivation of herpes simplex virus $\gamma_1$34.5 deletion mutants in rodent models. *J. Clin. Invest.* **91**, 2837–2843 (1993).
21. J. G. Spivack *et al.*, Replication, establishment of latent infection, expression of the latency-associated transcripts and explant reactivation of herpes simplex virus type 1 gamma 34.5 mutants in a mouse eye model. *J. Gen. Virol.* **76**, 321–332 (1995).
22. L. M. Robertson, A. R. MacLean, S. M. Brown, Peripheral replication and latency reactivation kinetics of the non-neurovirulent herpes simplex virus type 1 variant 1716. *J. Gen. Virol.* **73**, 967–970 (1992).
23. R. K. Mattila *et al.*, An investigation of herpes simplex virus type 1 latency in a novel mouse dorsal root ganglion model suggests a role for ICP34.5 in reactivation. *J. Gen. Virol.* **96**, 2304–2313 (2015).
24. M. van Gent, K. M. J. Sparrer, M. U. Gack, TRIM proteins and their roles in antiviral host defenses. *Annu. Rev. Virol.* **5**, 385–405 (2018).
25. A. Hage, R. Rajsbaum, To TRIM or not to TRIM: The balance of host-virus interactions mediated by the ubiquitin system. *J. Gen. Virol.* **100**, 1641–1662 (2019).
26. B. K. Ganser-Pornillos *et al.*, Hexagonal assembly of a restricting TRIM5alpha protein. *Proc. Natl. Acad. Sci. U.S.A.* **108**, 534–539 (2011).
27. T. Pertel *et al.*, TRIM5 is an innate immune sensor for the retrovirus capsid lattice. *Nature* **472**, 361–365 (2011).
28. D. Cuchet *et al.*, PML isoforms I and II participate in PML-dependent restriction of HSV-1 replication. *J. Cell Sci.* **124**, 280–291 (2011).
29. C. Cohen *et al.*, Promyelocytic leukemia (PML) nuclear bodies (NBs) induce latent/quiescent HSV-1 genomes chromatinization through a PML NB/Histone H3.3/H3.3 Chaperone Axis. *PLoS Pathog.* **14**, e1007313 (2018).
30. R. E. Watkinson, W. A. McEwan, J. C. Tam, M. Vaysburd, L. C. James, TRIM21 promotes cGAS and RIG-I sensing of viral genomes during infection by antibody-opsonized virus. *PLoS Pathog.* **11**, e1005253 (2015).
31. F. Full *et al.*, Centrosomal protein TRIM43 restricts herpesvirus infection by regulating nuclear lamina integrity. *Nat. Microbiol.* **4**, 164–176 (2019).
32. T. S. Reddi, P. E. Merkl, S. Y. Lim, N. L. Letvin, D. M. Knipe, Tripartite Motif 22 (TRIM22) protein restricts herpes simplex virus 1 by epigenetic silencing of viral immediate-early genes. *PLoS Pathog.* **17**, e1009281 (2021).
33. K. M. J. Sparrer *et al.*, TRIM23 mediates virus-induced autophagy via activation of TBK1. *Nat. Microbiol.* **2**, 1543–1557 (2017).
34. G. Fenteany *et al.*, Inhibition of proteasome activities and subunit-specific amino-terminal threonine modification by lactacystin. *Science* **268**, 726–731 (1995).
35. A. Vichi, D. M. Payne, G. Pacheco-Rodriguez, J. Moss, M. Vaughan, E3 ubiquitin ligase activity of the trifunctional ARD1 (ADP-ribosylation factor domain protein 1). *Proc. Natl. Acad. Sci. U.S.A.* **102**, 1945–1950 (2005).
36. K. Arimoto *et al.*, Polyubiquitin conjugation to NEMO by triparite motif protein 23 (TRIM23) is critical in antiviral defense. *Proc. Natl. Acad. Sci. U.S.A.* **107**, 15856–15861 (2010).
37. M. Laurent-Rolle *et al.*, The interferon signaling antagonist function of yellow fever virus NS5 protein is activated by type I interferon. *Cell Host Microbe* **16**, 314–327 (2014).
38. M. Watanabe *et al.*, The E3 ubiquitin ligase TRIM23 regulates adipocyte differentiation via stabilization of the adipogenic activator PPARγ. *eLife* **4**, e05615 (2015).
39. X. Liu, R. Matrenec, M. U. Gack, B. He, Disassembly of the TRIM23-TBK1 complex by the Us11 protein of herpes simplex virus 1 impairs autophagy. *J. Virol.* **93**, e00497-19 (2019).
40. D. Pan *et al.*, A neuron-specific host microRNA targets herpes simplex virus-1 ICP0 expression and promotes latency. *Cell Host Microbe* **15**, 446–456 (2014).
41. J. Chou, B. Roizman, The terminal a sequence of the herpes simplex virus genome contains the promoter of a gene located in the repeat sequences of the L component. *J. Virol.* **57**, 629–637 (1986).
42. E. M. McKay, B. McVey, H. S. Marsden, S. M. Brown, A. R. MacLean, The herpes simplex virus type 1 strain 17 open reading frame RL1 encodes a polypeptide of apparent M(r) 37K equivalent to ICP34.5 of herpes simplex virus type 1 strain F. *J. Gen. Virol.* **74**, 2493–2497 (1993).
43. H. Waisner, M. Kalamvoki, The ICP0 protein of herpes simplex virus 1 (HSV-1) downregulates major autophagy adaptor proteins sequestosome 1 and optineurin during the early stages of HSV-1 infection. *J. Virol.* **93**, e01258-19 (2019).
44. D. J. Royer *et al.*, A highly efficacious herpes simplex virus 1 vaccine blocks viral pathogenesis and prevents corneal immunopathology via humoral immunity. *J. Virol.* **90**, 5514–5529 (2016).
45. D. A. Leib *et al.*, Immediate-early regulatory gene mutants define different stages in the establishment and reactivation of herpes simplex virus latency. *J. Virol.* **63**, 759–768 (1989).
46. W. Cai *et al.*, The herpes simplex virus type 1 regulatory protein ICP0 enhances virus replication during acute infection and reactivation from latency. *J. Virol.* **67**, 7501–7512 (1993).
47. W. P. Halford, P. A. Schaffer, ICP0 is required for efficient reactivation of herpes simplex virus type 1 from neuronal latency. *J. Virol.* **75**, 3240–3249 (2001).
48. R. L. Thompson, N. M. Sawtell, Evidence that the herpes simplex virus type 1 ICP0 protein does not initiate reactivation from latency in vivo. *J. Virol.* **80**, 10919–10930 (2006).
49. R. Manivanh, J. Mehrbach, D. M. Knipe, D. A. Leib, Role of herpes simplex virus 1 gamma34.5 in the regulation of IRF3 signaling. *J. Virol.* **91**, e01156-17 (2017).
50. X. Liu, B. He, Selective editing of herpes simplex virus 1 enables interferon induction and viral replication that destroy malignant cells. *J. Virol.* **93**, e01761-18 (2019).
51. S. E. Conwell, A. E. White, J. W. Harper, D. M. Knipe, Identification of TRIM27 as a novel degradation target of herpes simplex virus 1 ICP0. *J. Virol.* **89**, 220–229 (2015).
52. V. Meza-Carmen *et al.*, Regulation of growth factor receptor degradation by ADP-ribosylation factor domain protein (ARD) 1. *Proc. Natl. Acad. Sci. U.S.A.* **108**, 10454–10459 (2011).
53. P. M. Ejercito, E. D. Kieff, B. Roizman, Characterization of herpes simplex virus strains differing in their effects on social behaviour of infected cells. *J. Gen. Virol.* **2**, 357–364 (1968).
54. Y. Ma *et al.*, Inhibition of TANK binding kinase 1 by herpes simplex virus 1 facilitates productive infection. *J. Virol.* **86**, 2188–2196 (2012).
55. Y. Kawaguchi, C. Van Sant, B. Roizman, Herpes simplex virus 1 alpha regulatory protein ICP0 interacts with and stabilizes the cell cycle regulator cyclin D3. *J. Virol.* **71**, 7328–7336 (1997).
56. Y. Kawaguchi *et al.*, Herpes simplex virus 1 alpha regulatory protein ICP0 functionally interacts with cellular transcription factor BMAL1. *Proc. Natl. Acad. Sci. U.S.A.* **98**, 1877–1882 (2001).
57. P. Mavromara-Nazos, M. Ackermann, B. Roizman, Construction and properties of a viable herpes simplex virus 1 recombinant lacking coding sequences of the alpha 47 gene. *J. Virol.* **60**, 807–812 (1986).
58. G. A. Versteeg *et al.*, The E3-ligase TRIM family of proteins regulates signaling pathways triggered by innate immune pattern-recognition receptors. *Immunity* **38**, 384–398 (2013).
59. Y. Wang *et al.*, p32 is a novel target for viral protein ICP34.5 of herpes simplex virus type 1 and facilitates viral nuclear egress. *J. Biol. Chem.* **289**, 35795–35805 (2014).
60. G. Cheng, M. E. Brett, B. He, Signals that dictate nuclear, nucleolar, and cytoplasmic shuttling of the $\gamma(_1)$34.5 protein of herpes simplex virus type 1. *J. Virol.* **76**, 9434–9445 (2002).
61. Y. Ma *et al.*, An engineered herpesvirus activates dendritic cells and induces protective immunity. *Sci. Rep.* **7**, 41461 (2017).
62. C. A. Schneider, W. S. Rasband, K. W. Eliceiri, NIH Image to ImageJ: 25 years of image analysis. *Nat. Methods* **9**, 671–675 (2012).
63. J. Schindelin *et al.*, Fiji: An open-source platform for biological-image analysis. *Nat. Methods* **9**, 676–682 (2012).